

SASHIMI-SIDM: Semi-analytical subhalo modelling for self-interacting dark matter at sub-galactic scales

Shin'ichiro Ando,^{a,b} Shunichi Horigome,^b Ethan O. Nadler,^{c,d}
Daneng Yang^e and Hai-Bo Yu^e

^aGRAPPA Institute, University of Amsterdam, Science Park 904, 1098 XH Amsterdam, The Netherlands

^bKavli Institute for the Physics and Mathematics of the Universe, University of Tokyo, Chiba 277-8583, Japan

^cCarnegie Observatories, 813 Santa Barbara Street, Pasadena, CA 91101, USA

^dDepartment of Physics & Astronomy, University of Southern California, Los Angeles, CA 90007, USA

^eDepartment of Physics and Astronomy, University of California, Riverside, CA 92521, USA

E-mail: s.ando@uva.nl

Abstract. We combine the semi-analytical structure formation model, SASHIMI, which predicts subhalo populations in collisionless, cold dark matter (CDM), with a parametric model that maps CDM halos to self-interacting dark matter (SIDM) halos. The resulting model, SASHIMI-SIDM, generates SIDM subhalo populations down to sub-galactic mass scales, for an arbitrary input cross section, in minutes. We show that SASHIMI-SIDM agrees with SIDM subhalo populations from high-resolution cosmological zoom-in simulations in resolved regimes. Crucially, we predict that the fraction of core-collapsed subhalos peaks at a mass scale determined by the input SIDM cross section and decreases toward higher halo masses, consistent with the predictions of gravothermal models and cosmological simulations. For the first time, we also show that the core-collapsed fraction decreases toward lower halo masses; this result is uniquely enabled by our semi-analytical approach. As a proof of principle, we apply SASHIMI-SIDM to predict the boost to the local dark matter density and annihilation rate from core-collapsed SIDM subhalos, which can be enhanced relative to CDM by an order of magnitude for viable SIDM models. Thus, SASHIMI-SIDM provides an efficient and reliable tool for scanning SIDM parameter space and testing it with astrophysical observations. The code is publicly available at <https://github.com/shinichiroando/sashimi-si>.

Contents

1	Introduction	1
2	Semi-analytical modelling of SIDM subhalos	2
2.1	SASHIMI for CDM	2
2.2	Parametric model of SIDM	4
2.3	SIDM models	6
2.4	Validity of SASHIMI in sub-resolution regimes	7
3	Model predictions and validations	8
3.1	Distribution of density profile parameters	8
3.2	Mass function and fraction of collapsed subhalos	8
3.3	Density profiles	11
4	Applications	12
4.1	Distinguishing SIDM models	12
4.2	Subhalo boost of dark matter annihilation	12
4.3	Probability distribution of dark matter density	13
5	Conclusions	16

1 Introduction

Dark matter accounts for more than 80% of the total matter in the Universe. Yet, its particle identity remains unknown, and understanding its properties as an elementary particle is a pressing task in physics. Whether the dark matter particles have non-gravitational interactions is one of the most intriguing questions one can tackle using modern astrophysical observations. In fact, various observations at sub-galactic scales indicate that the collisionless cold dark matter (CDM) scenario may not be complete, and that new physics may be needed, see, e.g., [1, 2]. As a compelling solution, self-interacting dark matter (SIDM), which was originally proposed to address the tensions between CDM predictions and observations of galactic systems [3], has attracted broad attention from multiple communities of particle physics, astrophysics, and cosmology; see [4, 5] for recent reviews.

In the SIDM scenario, dark matter particles can scatter with each other and exchange momentum. At the first stage of the gravothermal evolution of an SIDM halo, the heat is transported from the hotter outer region to the colder inner region, resulting in a flat density core towards the center, in contrast to a density cusp in CDM [6]. At the later stage, the inner region becomes hotter and the self-interactions transport heat outwards, leading to a high central density — a phenomenon called ‘gravothermal collapse’ [7, 8]. The collapse timescale depends on the self-interacting cross section per particle mass and the halo parameters, particularly, the halo concentration [9–11]. Therefore, SIDM predicts more diverse dark matter distributions in galaxies than CDM [11–18]. For satellite halos, environmental effects such as tidal stripping could further accelerate the onset of the collapse by lowering the temperature height of the halo [14, 19–23]. Thus, there is a novel interplay between gravitational evolution and tidal evolution for subhalos.

N-body simulations are leading tools to make SIDM predictions; see, e.g., [24–26] for recent work on subtleties of SIDM implementations in numerical simulations. Nevertheless, they are typically computationally expensive and less flexible in exploring a broad range of SIDM parameter space. Recently, ref. [18] proposed a parametric model for modelling SIDM halos and it is a semi-analytical method that can map CDM (sub)halos to their SIDM counterparts for a given particle physics realisation of SIDM. The model has been tested and validated using high-resolution cosmological simulations from ref. [27]. In this work, we further implement the parametric model into a semi-analytical tool for subhalo populations, **Semi-Analytical SubHalo Inference ModellIng** (SASHIMI).¹ SASHIMI is based on the theory of structure formation and it can compute CDM subhalo populations efficiently, avoiding issues related to numerical resolution and shot noise inevitable for simulation-based approaches. Being in good agreement with outcomes of cosmological CDM simulations such as subhalo mass functions [28] and distributions of subhalo density profile parameters [29], SASHIMI provides a reliable way to extend simulation results into sub-resolution regimes.

Here, we develop a new semi-analytical tool, SASHIMI-SIDM, for semi-analytically modelling SIDM subhalo populations. We will demonstrate that SASHIMI-SIDM predictions agree well with those from high-resolution cosmological SIDM simulations. For low-mass subhalos, one of our main findings is that the fraction of subhalos that are core-collapsed peaks at a mass scale determined by the SIDM cross section and decreases towards both higher and lower subhalo masses. As an application, we will evaluate the enhancement factors due to the collapse of SIDM subhalos for both direct and indirect detection experiments. For indirect detection, we find a boost for the rate of dark matter annihilation by up to an order of magnitude, with details depending on the SIDM model. Our method generates subhalo populations to be computed within minutes for a given host halo, will enable efficient scans over SIDM parameter space, and can be used to test regions of SIDM parameter space in a continuous manner. SASHIMI-SIDM is publicly available at <https://github.com/shinichiroando/sashimi-si>.

The rest of the paper is organised as follows. In section 2, we describe SASHIMI-SIDM by going over each model ingredient and discuss the model validity at sub-resolution scales. In section 3, we show various SASHIMI-SIDM outputs, including density profiles of cored and collapsed subhalos, subhalo mass function, and distribution of the density profile parameters. Furthermore, we validate our results using the corresponding simulation outputs, and then predict the subhalo populations in the sub-resolution regime. In section 4, we discuss applications of the subhalo populations with SASHIMI-SIDM for both direct and indirect detection experiments, and the dependence on SIDM models. We conclude in section 5. Throughout the paper, we adopt the following cosmological parameters: $H_0 = 100h$ km s⁻¹ Mpc⁻¹ with $h = 0.674$, $\Omega_m = 0.315$, and $\Omega_\Lambda = 0.685$. We use ‘ln’ to represent the natural logarithm, while ‘log’ is used for 10-based logarithm.

2 Semi-analytical modelling of SIDM subhalos

2.1 SASHIMI for CDM

SASHIMI is a publicly available numerical code for calculating various subhalo properties using semi-analytical models of structure formation [28]. SASHIMI computes the properties of CDM subhalos semi-analytically without being hindered by numerical resolutions or statistical noise. Given a host specified with its mass, redshift, and concentration parameter, it

¹See <https://github.com/shinichiroando/sashimi-c> for the CDM version of SASHIMI.

combines the accretion of CDM subhalos onto the host based on the extended Press-Schechter (ePS) formalism [30] with the modelling of subhalo evolution after accretion onto a host halo.

By adopting the ePS formalism, we could obtain the subhalo accretion rate per unit redshift z_a per unit subhalo mass m_a , $d^2N_{\text{sh}}/(dm_a dz_a)$. This quantity is represented as a function of (linearly extrapolated) critical over-density $\delta_c(z)$ of halo collapse at a given redshift z and mass variance $\sigma^2(m)$ for halo and subhalo masses m . The ePS formalism has been well calibrated against the numerical simulations (e.g., [31]). We refer the reader to refs. [28, 31] for detailed expressions of subhalo accretion rate $d^2N_{\text{sh}}/(dm_a dz_a)$.

Once the subhalo with the mass m_a accretes onto its host at z_a , it loses mass via tidal stripping. The following differential equation describes the mass evolution:

$$\dot{m}(z) = -A \frac{m(z)}{\tau_{\text{dyn}}(z)} \left[\frac{m(z)}{M(z)} \right]^\zeta, \quad (2.1)$$

where A and ζ are two parameters fitted against Monte Carlo simulations that are found to vary weakly as functions of M and z [28]. For the redshift evolution of the host mass $M(z)$, we adopt the result of ref. [32]. We solve eq. (2.1) with the initial condition of $m(z_a) = m_a$ to obtain the subhalo mass m at any redshift z between z_a and 0.

While the subhalo loses mass, its density profile is described by the Navarro-Frenk-White (NFW) function [6]:

$$\rho_{\text{CDM}}(r) = \frac{\rho_s}{(r/r_s)(r/r_s + 1)^2}, \quad (2.2)$$

where ρ_s is the density profile normalisation, r_s is the scale radius, and the profile is cut off abruptly beyond the tidal truncation radius r_t , which is obtained from mass conservation:

$$m = 4\pi \int_0^{r_t} dr r^2 \rho_{\text{CDM}}(r) = 4\pi \rho_s r_s^3 f\left(\frac{r_t}{r_s}\right). \quad (2.3)$$

We model the changes of r_s and ρ_s in terms of the related parameters r_{max} and V_{max} ,

$$r_s = \frac{r_{\text{max}}}{2.163}, \quad (2.4)$$

$$\rho_s = \frac{4.625}{4\pi G} \left(\frac{V_{\text{max}}}{r_s} \right)^2, \quad (2.5)$$

where V_{max} is the maximum circular velocity and r_{max} is the radius at which V_{max} is reached. The initial values of r_s and ρ_s at accretion are obtained via

$$m_a = \frac{4\pi}{3} \Delta_c(z_a) \rho_c(z_a) r_{\text{vir},a}^3, \quad (2.6)$$

$$r_{s,a} = \frac{r_{\text{vir},a}}{c_a}, \quad (2.7)$$

$$\rho_{s,a} = \frac{m_a}{4\pi r_{s,a}^3 f(c_{\text{vir},a})}, \quad (2.8)$$

where $\Delta_c = 18\pi^2 + 82d - 39d^2$ [33], $d = \Omega_m(1 + z_a)^3 / [\Omega_m(1 + z_a)^3 + \Omega_\Lambda] - 1$, $\rho_c(z_a)$ is the critical density of the Universe at z_a , and $f(c) = \ln(1 + c) - c/(1 + c)$. The virial concentration parameter c_a is generated following the log-normal distribution function with the mean $\bar{c}_{\text{vir}}(m_a, z_a)$ from refs. [32, 34], with appropriate conversions based on our halo mass definitions and a scatter of $\sigma_{\log c} = 0.13$ [35].

Following ref. [36], we parameterise the evolution of r_{\max} and V_{\max} after accretion as

$$\frac{V_{\max}}{V_{\max,a}} = \frac{2^{0.4}(m/m_a)^{0.3}}{(1+m/m_a)^{0.4}}, \quad (2.9)$$

$$\frac{r_{\max}}{r_{\max,a}} = \frac{2^{-0.3}(m/m_a)^{0.4}}{(1+m/m_a)^{-0.3}}. \quad (2.10)$$

Using eqs. (2.4) and (2.5) again, we obtain r_s and ρ_s at an arbitrary redshift $0 < z < z_0$.

2.2 Parametric model of SIDM

The parametric model of SIDM introduced in [18] connects parameters of an SIDM subhalo to the corresponding one in CDM. Once we know the evolution history of CDM subhalos and their density profile parameters, one can compute the SIDM counterpart following the prescription detailed in this subsection. We note, however, that we adopt the same ePS formalism $d^2 N_{\text{sh}}/(dm_a dz_a)$ as in the case of CDM. This is based on two assumptions: (i) the linear power spectrum is unchanged between CDM and SIDM (i.e., we only consider “late-time” effects of SIDM), and (ii) self-interactions generally have a minor impact on halo abundances and orbital properties before infall [27, 37]. The second assumption should be revisited carefully for models that reach very large cross sections (e.g., [11]).

For the density profile of the SIDM subhalos, we adopt the following parameterisation:

$$\rho_{\text{SIDM}}(r) = \frac{\rho_s}{[(r^\beta + r_c^\beta)^{1/\beta}/r_s](r/r_s + 1)^2}, \quad (2.11)$$

up to the tidal truncation radius r_t , beyond which the density decreases quickly (for a more accurate treatment of the cutoff, see [18]). In eq. (2.11), r_c is the core radius within which the density profile is flat. We adopt $\beta = 4$ throughout this work. Instead of directly using (ρ_s, r_s, r_c) , we work in the basis of (V_{\max}, r_{\max}) and then convert to these parameters. Following the integral model approach of ref. [18], these parameter sets of SIDM can be obtained from the density profile parameters of CDM through the relation:

$$V_{\max}^{\text{SIDM}}(t) = V_{\max}^{\text{CDM}}(t) + \int_{t_f}^t \frac{dt'}{t_c(t')} \frac{dV_{\max, \text{Model}}(\tilde{t}')}{d\tilde{t}'}, \quad (2.12)$$

$$r_{\max}^{\text{SIDM}}(t) = r_{\max}^{\text{CDM}}(t) + \int_{t_f}^t \frac{dt'}{t_c(t')} \frac{dr_{\max, \text{Model}}(\tilde{t}')}{d\tilde{t}'}, \quad (2.13)$$

$$\begin{aligned} \frac{dV_{\max, \text{Model}}(\tilde{t})}{d\tilde{t}} &= V_{\max}^{\text{CDM}}(t_f) [0.1777 - 4.399(3\tilde{t}^2) + 16.66(4\tilde{t}^3) - 18.87(5\tilde{t}^4) \\ &\quad + 9.077(7\tilde{t}^6) - 2.436(9\tilde{t}^8)] \Theta(1.1 - \tilde{t}), \end{aligned} \quad (2.14)$$

$$\frac{dr_{\max, \text{Model}}(\tilde{t})}{d\tilde{t}} = r_{\max}^{\text{CDM}}(t_f) [0.007623 - 0.7200(2\tilde{t}) + 0.3376(3\tilde{t}^2) - 0.1375(4\tilde{t}^3)] \Theta(1.1 - \tilde{t}), \quad (2.15)$$

where t_f is the time when the given subhalo is formed, $\tilde{t} = (t - t_f)/t_c(t)$, $t_c(t)$ is the core-collapse timescale (defined below), and Θ is the Heaviside step function. The second term of the right-hand side of eqs. (2.12) and (2.13) takes the SIDM effects into account such as core formation and collapse, while the first term is obtained as a result of the tidal effects. By using the step function Θ , we terminate the SIDM effect (i.e., the second term) once

the collapse phase has been reached, $\tilde{t} > 1.1$, up to which the parametric model has been calibrated against N-body simulations [18].

The conversion from (V_{\max}, r_{\max}) to (ρ_s, r_s, r_c) for SIDM subhalos can be implemented as follows. Firstly, starting with $V_{\max}^{\text{SIDM}}(t)$ and $r_{\max}^{\text{SIDM}}(t)$ obtained above, we compute $V_{\max,0}^{\text{CDM}}$ and $r_{\max,0}^{\text{CDM}}$ using the following relations:

$$\frac{V_{\max}^{\text{SIDM}}(t)}{V_{\max,0}^{\text{CDM}}} = 1 + 0.1777\tilde{t} - 4.399\tilde{t}^3 + 16.66\tilde{t}^4 - 18.87\tilde{t}^5 + 9.077\tilde{t}^7 - 2.436\tilde{t}^9, \quad (2.16)$$

$$\frac{r_{\max}^{\text{SIDM}}(t)}{r_{\max,0}^{\text{CDM}}} = 1 + 0.007623\tilde{t} - 0.7200\tilde{t}^2 + 0.3376\tilde{t}^3 - 0.1375\tilde{t}^4. \quad (2.17)$$

For the subhalos which have reached the collapsing phase, we adopt $\tilde{t} = 1.1$. $V_{\max,0}^{\text{CDM}}$ and $r_{\max,0}^{\text{CDM}}$ are the initial values of these parameters of a *fictitious* CDM halo. Secondly, we convert $(V_{\max,0}^{\text{CDM}}, r_{\max,0}^{\text{CDM}})$ to $(\rho_{s,0}^{\text{CDM}}, r_{s,0}^{\text{CDM}})$ using eqs. (2.4) and (2.5) for the same fictitious CDM halo. Finally, using

$$\frac{\rho_s^{\text{SIDM}}(t)}{\rho_{s,0}^{\text{CDM}}} = 2.033 + 0.7381\tilde{t} + 7.264\tilde{t}^5 - 12.73\tilde{t}^7 + 9.915\tilde{t}^9 + (1 - 2.033) \frac{\ln(\tilde{t} + 0.001)}{\ln 0.001}, \quad (2.18)$$

$$\frac{r_s^{\text{SIDM}}(t)}{r_{s,0}^{\text{CDM}}} = 0.7178 + 0.1026\tilde{t} + 0.2474\tilde{t}^2 - 0.4079\tilde{t}^6 + (1 - 0.7178) \frac{\ln(\tilde{t} + 0.001)}{\ln 0.001}, \quad (2.19)$$

$$\frac{r_c^{\text{SIDM}}(t)}{r_{s,0}^{\text{CDM}}} = 2.555\sqrt{\tilde{t}} - 3.632\tilde{t} + 2.131\tilde{t}^2 - 1.415\tilde{t}^3 + 0.4683\tilde{t}^4, \quad (2.20)$$

we compute the density profile parameters of the SIDM subhalo at time t .

We adopt the formation redshift z_f from ref. [32]:

$$z_f = -0.0064[\log(m_{\text{vir},0}/M_{\odot})]^2 + 0.0237 \log(m_{\text{vir},0}/M_{\odot}) + 1.8837, \quad (2.21)$$

where $m_{\text{vir},0}$ is the extrapolated subhalo's virial mass at present ($z = 0$), if there were no tidal processes or SIDM effects. To connect the virial mass at accretion m_a and at present $m_{\text{vir},0}$, we adopt eq. (19) of ref. [32]. The formation time t_f is then computed as

$$t_f = \frac{1}{H_0} \int_{z_f}^{\infty} \frac{dz}{(1+z)\sqrt{\Omega_m(1+z)^3 + \Omega_{\Lambda}}}, \quad (2.22)$$

and the lookback time corresponding to z_f is $t_L(z_f) = t_U - t_f$, where $t_U \approx 13.8$ Gyr is the age of the Universe.

Finally, the core-collapse timescale, t_c , can be expressed as [7, 38]

$$t_c = \frac{150}{C(\sigma_{\text{eff}}/m_{\chi})\rho_s^{\text{CDM}}r_s^{\text{CDM}}} \frac{1}{\sqrt{4\pi G\rho_s^{\text{CDM}}}}, \quad (2.23)$$

where $C = 0.75$ [8, 9, 19, 39]. This timescale is a function of the cosmic time t , through the evolving density profile parameters ρ_s^{CDM} and r_s^{CDM} as well as the effective scattering cross section per SIDM particle mass, $(\sigma_{\text{eff}}/m_{\chi})$. We introduce this effective cross section and our SIDM models in the following subsection.

	σ_0/m_χ [$\text{cm}^2 \text{g}^{-1}$]	w [km s^{-1}]
Model I	147.1	24.33
Model II	2.4×10^4	1
Model III	147.1	120
Model IV	5	100
Model V	10	–

Table 1. SIDM model parameters. Model I is adopted as our fiducial model [16, 27], and used throughout the work, including to compare SASHIMI-SIDM predictions with cosmological simulation results [27]. The other models are discussed in Section 4.1. Model III was simulated in ref. [11], and Model V is a velocity-independent case chosen for illustrative purposes.

To summarise, we use Eqs. (2.12)–(2.15) to obtain $(V_{\text{max}}, r_{\text{max}})$ for SIDM from those for CDM, and convert them to (ρ_s, r_s, r_c) for SIDM via Eqs. (2.16)–(2.20). As the parameters (ρ_s, r_s) of the CDM density profile at any redshifts are entirely determined by (m_a, z_a, c_a) , we can also obtain (ρ_s, r_s, r_c) for SIDM in a deterministic manner once we specify (m_a, z_a, c_a) . In other words, we have complete functional forms for any parameters of the subhalo density profile that depends only on (m_a, z_a, c_a) : $\theta = \theta(m_a, z_a, c_a)$.

2.3 SIDM models

We consider the velocity-dependent scattering cross section

$$\frac{d\sigma}{d\cos\theta} = \frac{\sigma_0}{2[1 + (v/w)^2 \sin^2(\theta/2)]^2}, \quad (2.24)$$

which is characterised by two parameters: the cross section amplitude σ_0 , and the velocity scale of the transition between velocity-dependent and velocity-independent scattering, w . As default values, we adopt $\sigma_0/m_\chi = 147.1 \text{ cm}^2 \text{g}^{-1}$ and $w = 24.33 \text{ km s}^{-1}$ [16, 27] for most of the present paper.

In figure 1, we show the ‘viscosity’ scattering cross section [40] after integrating eq. (2.24) over $\cos\theta$ with the weight of $3 \sin^2\theta/2$:

$$\sigma_V = \frac{6\sigma_0 w^4}{v^4} \left[\left(1 + \frac{2w^2}{v^2}\right) \ln \left(1 + \frac{v^2}{w^2}\right) - 2 \right], \quad (2.25)$$

for this and other models from the previous literature [11, 18, 41]; we summarise the SIDM parameters of these models in table 1. Along with four velocity-dependent SIDM models (Models I, II, III, and IV), we also consider a velocity-independent model with $\sigma_0/m_\chi = 10 \text{ cm}^2 \text{g}^{-1}$ for illustrative purposes only, since observations on galaxy cluster scales imply $\sigma_0/m_\chi < 0.1 \text{ cm}^2 \text{g}^{-1}$ for velocity-independent scattering [42, 43].

The viscosity cross section is suggested as a better representation of an angle-integrated quantity than the total cross section $\sigma_{\text{total}} = \sigma_0/(1 + v^2/w^2)^2$ [40]. The effective cross section σ_{eff} is obtained by [39, 40]

$$\sigma_{\text{eff}} = \frac{1}{512v_{\text{eff}}^8} \int_0^\infty dv \int_{-1}^1 d\cos\theta \frac{d\sigma}{d\cos\theta} v^7 \sin^2\theta \exp \left[-\frac{v^2}{4v_{\text{eff}}^2} \right], \quad (2.26)$$

which depends on subhalo density profile via $v_{\text{eff}} = 0.64V_{\text{max}}^{\text{CDM}}$ [44].

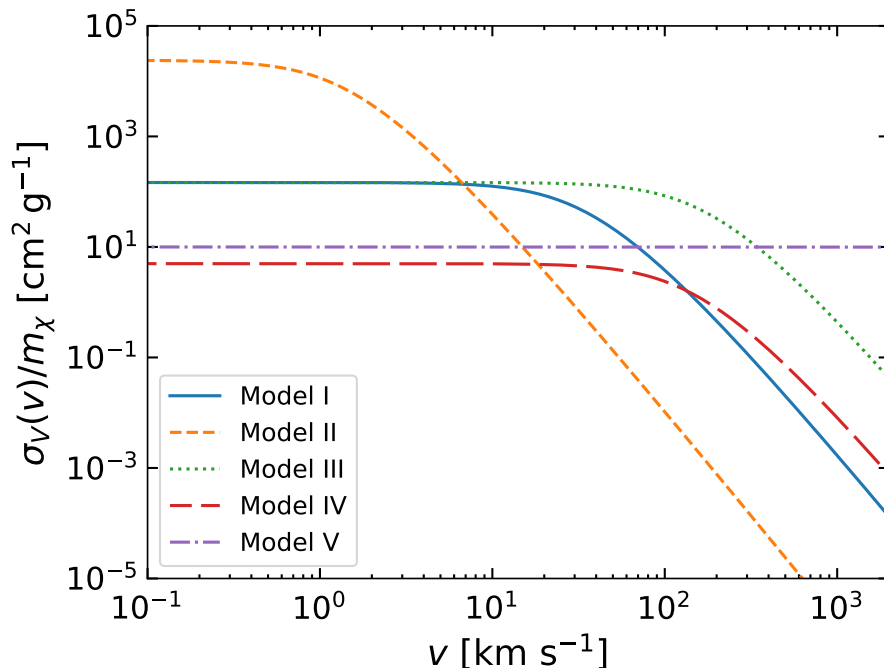


Figure 1. Viscosity cross section per unit dark matter mass, σ_V/m_χ , as a function of relative velocity for five benchmark SIDM models. Our fiducial SIDM model (Model I) with $\sigma_0/m_\chi = 147.1 \text{ cm}^2 \text{ g}^{-1}$ and $w = 24.33 \text{ km s}^{-1}$ [16, 27] is adopted throughout the paper, while the other models (table 1) are discussed in Section 4.1. Model III was simulated in ref. [11], and Model V is a velocity-independent scenario for illustrative purposes.

2.4 Validity of SASHIMI in sub-resolution regimes

One of the advantages of adopting semi-analytical models like SASHIMI over approaches based on numerical simulations is that they are free from issues related to numerical resolution in cosmological simulations. If the physical ingredients such as our ePS formalism and parametric SIDM model are assumed to be valid, then our SASHIMI-SIDM predictions will be trustworthy. We may therefore make predictions for arbitrarily small subhalos under this assumption. Before doing so, we will demonstrate in Section 3 that SASHIMI-SIDM matches the predictions of cosmological SIDM simulations in resolved regimes.

The ePS formalism has been tested and proven to be a valid tool across a wide range of masses, redshifts, and environments (e.g., [45]). The parametric model for SIDM discussed in Section 2.2 depends on the cosmic time since the subhalos' formation, normalized by the collapse timescale. The collapse timescale depends on the scattering cross section (per unit dark matter mass) and halo density profile parameters, and thus our ansatz is that this dependence continues to hold at much smaller scales. This, however, must be tested against future numerical simulations with higher resolution.

Below, we provide the first direct comparison between SASHIMI-SIDM predictions and high-resolution zoom-in cosmological simulations of SIDM. In order to do so and also to make predictions for various observables, we will make appropriate cuts in the following sections.

3 Model predictions and validations

Using SASHIMI, we generate a list of subhalos in a Milky Way-mass host with $M_{200} = 10^{12} M_{\odot}$ at $z = 0$. The parameters related to the subhalo's density profile are mass at both accretion and at present ($z = 0$), redshift at accretion z_a , ρ_s and r_s for both CDM and SIDM, the core radius r_c for SIDM, and the tidal truncation radius r_t .

The properties of each subhalo are entirely characterised by three parameters m_a , z_a , and c_a , throughout its evolution history. We generate these quantities following their distributions; i.e., the ePS $d^2 N_{\text{sh}}/(dm_a dz_a)$ for the former two, and the log-normal distribution $P(c_a)$ for the latter. We assign each subhalo entry in the list a weight factor, i.e., the ensemble average of the number of such a subhalo: $w_i = \langle N_{\text{sh},i} \rangle$. This approximates the distribution of (m_a, z_a, c_a) as

$$\int dz_a \int dm_a \frac{d^2 N_{\text{sh}}}{dm_a dz_a} \int dc_a P(c_a | \bar{c}_{\text{vir}}(m_a, z_a), \sigma_{\log \sigma}) \longrightarrow \sum_i w_i. \quad (3.1)$$

We then generate the distribution function of any combination of subhalo parameters, θ ,

$$\frac{dN_{\text{sh}}}{d\theta} = \int dz_a \int dm_a \frac{d^2 N_{\text{sh}}}{dm_a dz_a} \int dc_a P(c_a | \bar{c}_{\text{vir}}(m_a, z_a), \sigma_{\log c}) \delta_D(\theta - \theta(m_a, z_a, c_a)), \quad (3.2)$$

by making a (multi-dimensional) histogram with weights w_i .

3.1 Distribution of density profile parameters

Figure 2 shows the density contour in the two-dimensional parameter space: $\theta = (V_{\text{max}}, r_{\text{max}})$, computed using eq. (3.2). The top panels are for the subhalos with the masses within the truncation radius at $z = 0$ that are larger than $10^8 M_{\odot}/h$. We compare the distributions in the case of SIDM with that of CDM. We also plot results from cosmological zoom-in simulations of SIDM Model I, presented in the previous study by some of the present authors [18], as green data points. Our SASHIMI-SIDM predictions broadly agree with these simulation results for both the CDM and SIDM cases. We leave a detailed statistical analysis based on matching individual subhalos in cosmological simulations to future work.

In the bottom panels of figure 2, we extend the SASHIMI-SIDM predictions to the sub-resolution regime with the subhalo mass threshold of $10^6 M_{\odot}/h$. The resulting r_{max} distribution extends to much lower values compared to the top panel, while the V_{max} distribution hardly changes. This follows because the rotation curves of collapsed SIDM subhalos reach a similar maximum velocity at a much smaller radius, reflecting their higher concentration.

Figure 3 shows a subhalo population generated by Monte-Carlo sampling the SASHIMI-SIDM prediction with $\theta = (V_{\text{max}}, r_{\text{max}})$ and (r_s, r_c) , in the left and right panels, respectively. The colour of these scattered points shows the lookback time to the subhalo formation redshift $t_L(z_f)$ in units of the collapse timescale t_c . The subhalos in the collapsing phase, $t_L(z_f)/t_c \approx 1$, show substantially smaller r_{max} values for the same V_{max} values. The core radius r_c is strongly correlated with the scale radius r_s . The relation saturates around $r_s \approx 5r_c$ for the subhalos in the core-collapse phase.

3.2 Mass function and fraction of collapsed subhalos

We discuss the subhalo mass function, for which $\theta = m$ is the present-day bound subhalo mass. In figure 4 (left), we show dN_{sh}/dm for the subhalos. We also show the mass function

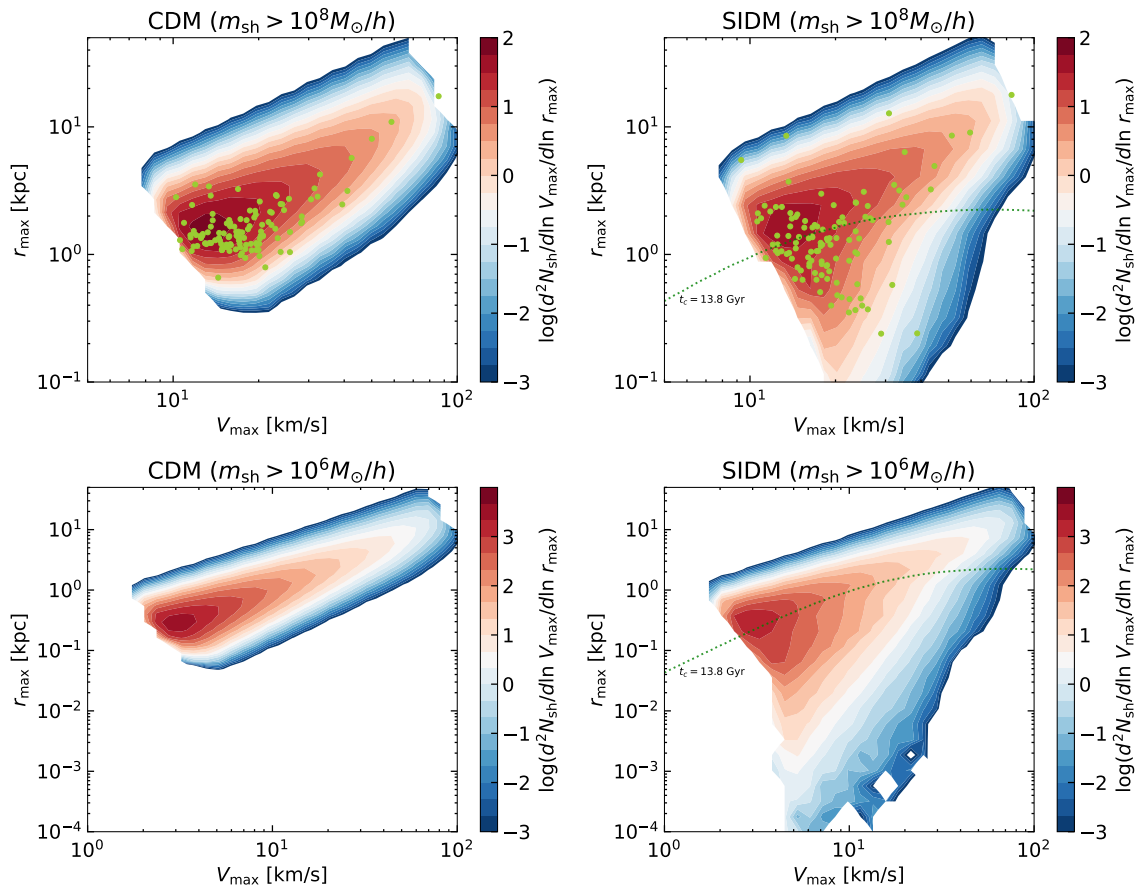


Figure 2. Subhalo number distribution in the (V_{\max}, r_{\max}) parameter space for CDM (*left*) and SIDM (*right*) for the SIDM Model I (table 1). The subhalos shown have masses larger than $10^8 M_{\odot}/h$ (*top*) and $10^6 M_{\odot}/h$ (*bottom*). Green data points in the top panels are from cosmological zoom-in simulations of SIDM Model I [18]. The dotted curve in each panel shows a contour of the collapse timescale, obtained by setting t_c from eq. (2.23) equal to the age of the Universe, 13.8 Gyr. The SIDM subhalos below this curve are expected to be in core-collapse phase at $z = 0$.

of the subhalos that have already collapsed with $t_L(z_f)/t_c > 1, 2, \text{ and } 3$. The fraction of collapsed subhalos is shown in the right panel. The subhalo mass function is hardly changed compared to that of the CDM case. This is based on the assumption that the ePS formalism does not change, and that the subhalo masses are not significantly affected by self-interactions (e.g., [27]). Strikingly, the fraction of core-collapsed subhalos with $t_L(z_f)/t_c > 1$ peaks at $\sim 30\%$ for the subhalos with the masses of $10^7\text{--}10^8 M_{\odot}$.

We can understand this result analytically as follows. The mass scale where the core-collapsed fraction peaks is determined by the underlying SIDM cross section and the mass-concentration relation. We parameterize the velocity dependence of the effective cross section as $\sigma_{\text{eff}} \propto \sigma_0 v^{-n}$, where the power-law exponent n is a number varying from 0 to 4 in our SIDM scenarios. For a given halo, $v \sim V_{\max} \propto (\rho_s^{\text{CDM}})^{1/2} r_s^{\text{CDM}}$. Hence, from eq. (2.23), we see that the core-collapse timescale scales as

$$t_c \propto \frac{1}{(\sigma_{\text{eff}}/m_{\chi}) r_s^{\text{CDM}} (\rho_s^{\text{CDM}})^{3/2}} \propto (\sigma_0/m_{\chi})^{-1} m^{(n-1)/3} c^{(n-7)/2}, \quad (3.3)$$

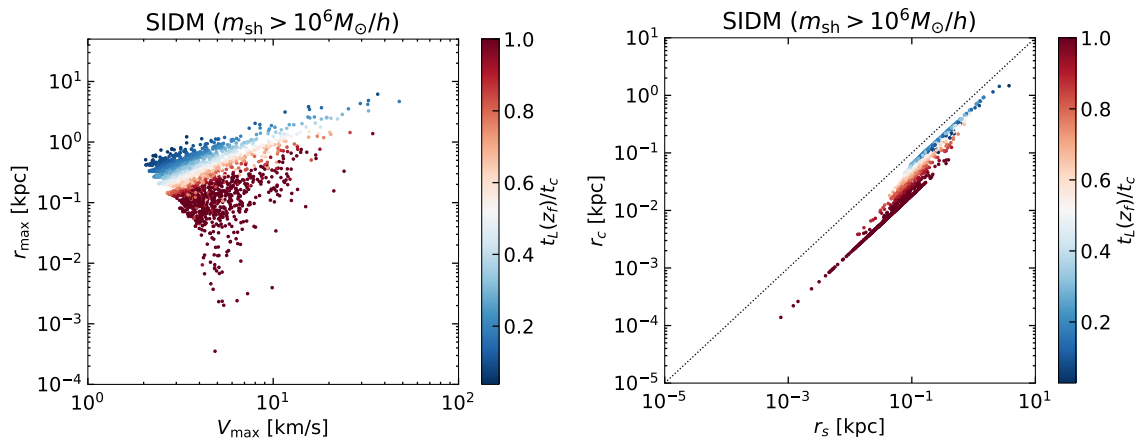


Figure 3. A realisation of a SASHIMI-SIDM subhalo population with masses heavier than $10^6 M_\odot/h$, on the (V_{\max}, r_{\max}) (*left*) and (r_s, r_c) (*right*) planes for the SIDM Model I. The diagonal dotted line in the right panel show the one-to-one $r_c = r_s$ relation. The colour corresponds to the lookback time to the subhalo formation redshift, $t_L(z_f)$, in units of the collapse timescale t_c . The colours are saturated for all the subhalos in the core-collapse phase, $t_L(z_f)/t_c > 1$, as the evolution has been stopped once it reaches $t_L(z_f)/t_c = 1.1$.

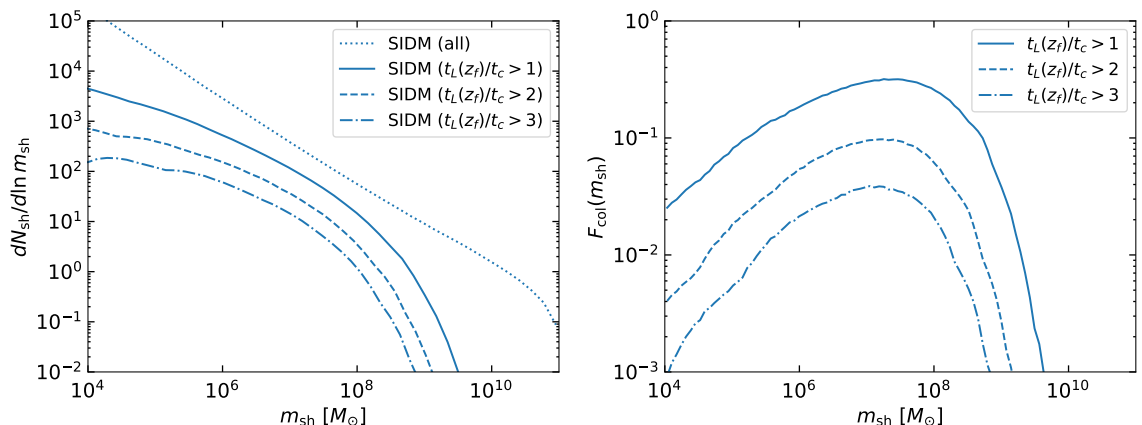


Figure 4. *Left:* Subhalo mass function for the SIDM Model I, which is nearly identical to CDM. The mass function of the collapsed subhalos with $t_L(z_f)/t_c > 1, 2$, and 3 are also shown. *Right:* Collapse fraction F_{col} : i.e., the ratio of mass functions of collapsed subhalos compared to the total population.

where we have used the scaling relations $\rho_s^{\text{CDM}} \propto c^3$ and $r_s^{\text{CDM}} \propto m^{1/3}/c$. In the limit $n = 0$, $t_c \propto (\sigma/m_\chi)^{-1} m^{-1/3} c^{-7/2}$ [9, 11].

According to our assumed mass–concentration relation from ref. [34], $c \propto m^{-0.036}$ in the low-mass regime. Thus, for halos that probe the velocity-independent part of the SIDM cross section ($n = 0$), $t_c \propto m^{-0.2}$, implying that the core-collapsed fraction decreases toward lower halo masses. Meanwhile, for halos in the velocity-dependent regime of the cross section ($n = 4$), $t_c \propto m^{1.1}$ and higher-mass halos collapse more slowly. In the context of our SIDM parameterisation, the amplitude of the core-collapse fraction peak is set by σ_0 , and the mass scale of the peak is set by w . For SIDM Model I, the core-collapse fraction peaks at $\approx 30\%$, consistent with cosmological zoom-in simulation results for this model [27]. This

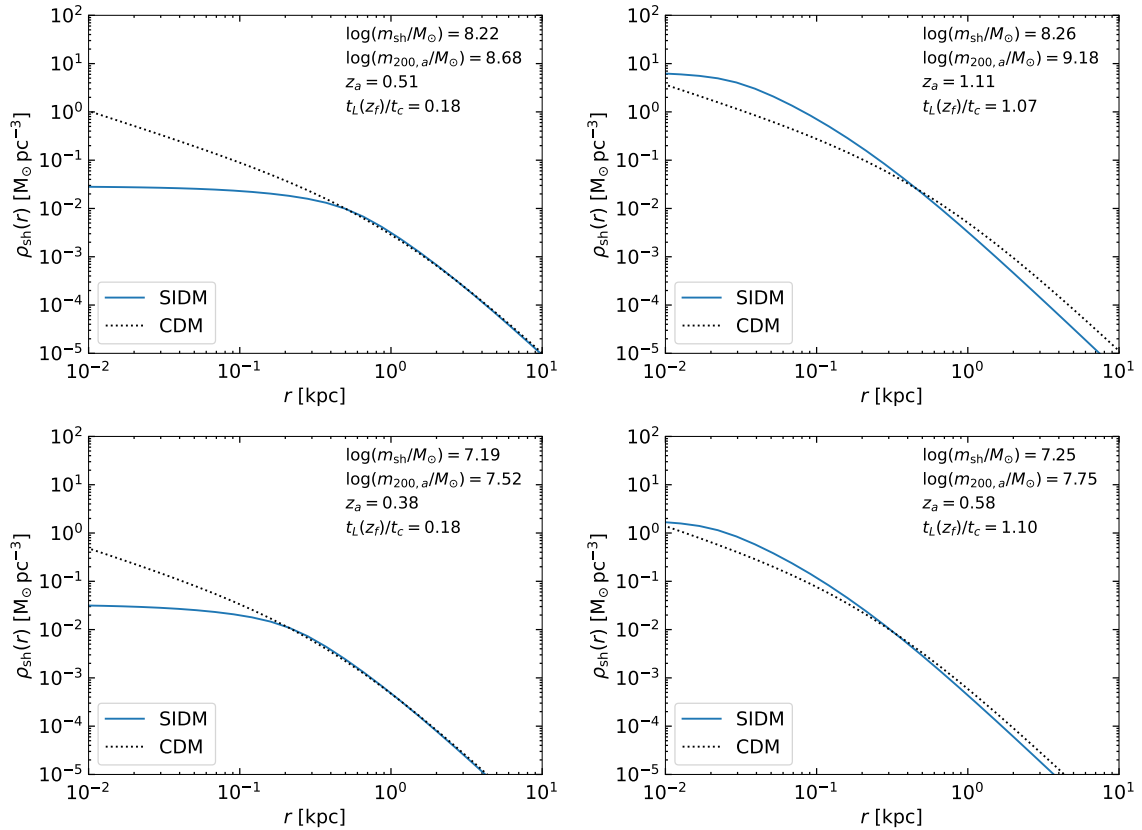


Figure 5. Density profiles of both CDM and SIDM subhalos with the parameters shown: the present bound mass m_{sh} , mass at accretion $m_{200,a}$, redshift at accretion z_a , and the lookback time of the subhalo formation $t_L(z_f)$ in units of collapse timescale t_c . The left panels show subhalos in a core-forming phase ($t_L(z_f)/t_c \sim 0.2$), and the right panels show those in a collapsing phase ($t_L(z_f)/t_c \gtrsim 1$).

peak occurs for $\approx 10^8 M_\odot$ subhalos, which have maximum circular velocities comparable to the $w = 24.33 \text{ km s}^{-1}$ in this model. In Section 4.1, we present core collapse fractions for other SIDM models to expand on these predictions and confirm the dependence of the core-collapse fraction on σ_0 and w .

3.3 Density profiles

We demonstrate several examples of subhalos' density profiles, shown in figure 5. These subhalos were randomly sampled following the subhalo distribution generated with SASHIMI-SIDM under conditions of $t_L(z_f)/t_c \approx 0.18$ (left panels) and $t_L(z_f)/t_c \approx 1.1$ (right panels). We chose subhalos, whose masses fall within a 10^7 – $10^9 M_\odot$ range, for the core-forming and core-collapsed cases.

As expected, if the core-collapse timescale t_c is shorter than the lookback time corresponding to the halo formation $t_L(z_f)$, the subhalo is in the core-collapse phase. To make our predictions conservative (i.e., such that we underestimate the density of the collapsed subhalos), we stop our calculations and freeze the density profile evolution according to the SIDM effects once the subhalo reaches $t_L(z_f)/t_c = 1.1$. We note that the subhalos will keep evolving after reaching the collapsing time t_c and might form a black hole at the subhalo centre in extreme scenarios (e.g., [46]).

4 Applications

We apply the SASHIMI-SIDM results to predict a few observables to probe the particle properties of dark matter using future experiments and observations. More detailed analyses are slated for several follow-up studies. Here, we demonstrate a couple of simple examples of applications.

4.1 Distinguishing SIDM models

First, we discuss the dependence on the SIDM parameters σ_0/m_χ and w . The left panel of figure 6 shows the fraction of collapsed subhalos with $t_L(z_f)/t_c > 1$ as a function of the subhalo mass. The parameters and cross sections of these SIDM models are as shown in table 1 and figure 1, respectively. As expected, the larger the cross section σ_0 is, so is the collapse fraction. The velocity scale w , which sets the transition scale from $\sigma_0 \propto v^0$ to $\propto v^{-4}$, decides the mass scales of the core-collapsed subhalos. Particularly for SIDM Model II, which saturates at the large value of $\sigma_0/m_\chi = 2.4 \times 10^4 \text{ cm}^2 \text{ g}^{-1}$, nearly all the subhalos with the masses of $1\text{--}10^6 M_\odot$ collapse.

We emphasize that, in the subhalo mass regime where simulations can resolve core collapse, these results are consistent with previous studies [11, 27, 47]. However, our semi-analytical approach allows us to predict the core-collapse fraction down to very low subhalo masses and to reveal its turnover. It will be interesting to design cosmological simulations that capture this turnover in future work. Future surveys of Milky Way dwarf galaxies and follow-up measurements of their dark matter density profiles will help determine the population of dwarfs that are potentially in the collapse phase. They may further help distinguish different SIDM models, where our method provides essential tools.

4.2 Subhalo boost of dark matter annihilation

Next, we discuss a possibility that the SIDM particles self-annihilate into Standard Model final states (motivated by several particle physics models, e.g., [48, 49]). Since the rate of self-annihilation depends on the density squared, the subhalos in the core-collapse phase will enhance the annihilation signal, and this signature will depend on the SIDM model parameters through the core-collapsed fraction. We estimate the total luminosity of Standard Model particles such as photons from the dark matter annihilation in all the subhalos with

$$L_{\text{sh,tot}} \propto \sum_i w_i \int dr 4\pi r^2 \rho_{\text{sh},i}^2(r). \quad (4.1)$$

By dividing this quantity by the luminosity of the main halo component by assuming the NFW profile (i.e., CDM without subhalos), we define the annihilation boost factor: $B_{\text{sh}} \equiv L_{\text{sh,tot}}/L_{\text{host,NFW}}^0$. We then compare this quantity for CDM and SIDM, and investigate the dependence on the subhalo masses considered. Our assumption that the main halo is CDM-like is reasonable even for our SIDM models because baryons contract the inner host halo [50–53]. This choice allows us to isolate the effects of SIDM on subhalo populations. We note that the effect of sub-subhalos and finer structures is not included in the following calculations, and hence the results in this subsection is conservative.

The right panel of figure 6 shows the annihilation boost factor due to the subhalos more massive than a threshold mass $m_{\text{sh}}^{\text{th}}$, $B_{\text{sh}}(> m_{\text{sh}}^{\text{th}})$. First, we focus on comparing SIDM Model I to CDM. As we include smaller subhalos, the CDM boost factor gradually increases and exceeds 1 for $m_{\text{sh}} > M_\odot$ [28, 54]. On the other hand, for the SIDM model, the contribution

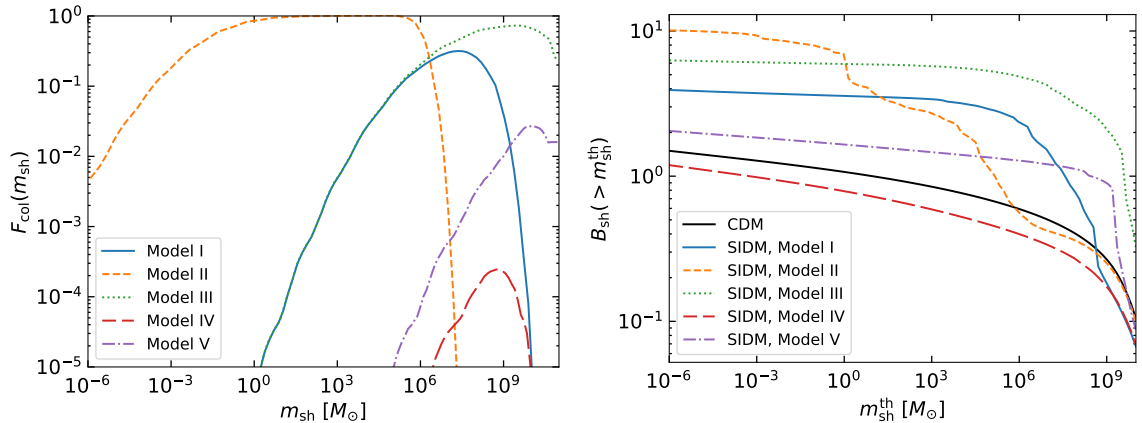


Figure 6. *Left:* Core-collapsed fractions (same as figure 4 right panel, $t_L(z_f)/t_c > 1$), for various SIDM models. *Right:* The annihilation boost factor — the ratio of the luminosity from dark matter annihilation in the subhalos and the CDM smooth host halo — as a function of threshold subhalo mass $m_{\text{sh}}^{\text{th}}$. For the parameters of SIDM models, see table 1.

from subhalos with masses larger than $\sim 10^8 M_\odot$ is small as many of them are cored. A clear transition happens once the subhalos with masses smaller than $\sim 10^8 M_\odot$ are included. Because of the large population of core-collapsed subhalos ($t_L(z_f)/t_c > 1$) that have much steeper profile than the CDM case, the signals of dark matter annihilation are boosted up to a factor of 4. Given the null observations of dark matter annihilation in any existing gamma-ray data, the model will be stringently constrained by using the existing gamma-ray data from the Milky Way halo, dwarf spheroidal galaxies [29, 55], unassociated Fermi sources, clusters of galaxies, and unresolved gamma-ray background. More careful analyses of these targets are the subject for our future study.

SIDM models that predict larger fraction of collapsed subhalos yield more conspicuous dark matter annihilation boosts. In particular, for SIDM Model II, the boost factor reaches $B_{\text{sh}} \sim 10$ but only if the halos with masses smaller than $1 M_\odot$ exist. For SIDM Model III, the larger subhalos with $m_{\text{sh}} > 10^9 M_\odot$ could collapse within the Hubble time, and thus enhance the boost factor substantially.

4.3 Probability distribution of dark matter density

What is the dark matter density at a given point in the Galaxy? This is one of the most relevant questions for dark matter direct detection experiments. It may also have some relevance for several gravitational probes, such as gravitational lensing, gaps in stellar streams, and pulsar timing arrays. To this end, we predict the probability density function $P(\rho) = dP/d\rho$ of dark matter density at a given radius (e.g., $r = 8$ kpc for the solar system), $\rho(r) = \rho_{\text{sh}}(r) + \rho_{\text{h}}(r)$, where ρ_{sh} and ρ_{h} are the subhalo and host halo components, respectively. This is motivated by several earlier studies [56–58].

Suppose we are in a dark matter subhalo i , which subtends to its truncation radius $r_{t,i}$. Then, the conditional probability of finding a subhalo density between ρ_{sh} and $\rho_{\text{sh}} + d\rho_{\text{sh}}$, $P(\rho_{\text{sh}}|i)d\rho_{\text{sh}}$ is obtained via

$$P(\rho_{\text{sh}}|i)d\rho_{\text{sh}} = \left| \frac{dP_{\text{sh},i}}{dr} \right| \left| \frac{dr}{d\rho_{\text{sh},i}} \right| \propto \frac{r^2}{|d\rho_{\text{sh},i}/dr|}, \quad (4.2)$$

where $P_{\text{sh},i}$ after the first equality is the probability of finding the point of interest at a radius r from the subhalo centre, which goes as $dP_{\text{sh},i}/dr \propto r^2$. The denominator of the last expression $|d\rho_{\text{sh},i}/dr|$ can be evaluated using the density profile expressions for either the CDM or SIDM case, in eqs. (2.2) and (2.11), respectively.

The volume of subhalo i is $V_{\text{sh},i} = 4\pi r_{t,i}^3/3$. We assume that the subhalos' spatial distribution follows the density function $n_{\text{sh}}(r) \propto \exp[(2/\alpha)(r/r_{-2})^\alpha]$ independent of the mass, where $\alpha = 0.678$, $r_{-2} = 0.81r_{200}$, and r_{200} is the radius within which the average density is 200 times the critical density [59]. With this assumption, the probability per volume that a random subhalo is located at the radius r from the halo centre, $P_{\text{sh},V}$, is proportional to $n_{\text{sh}}(r)$. Therefore, at the radius r , the probability of finding a subhalo i at our location is $P(i) = w_i V_{\text{sh},i} P_{\text{sh},V}$. Note that the weight factor w_i is needed as i represents a collection of the subhalos specified with the same parameters, whose total number is w_i . Combined with the conditional probability from eq. (4.2), the total probability density function for ρ_{sh} is

$$P_{\text{sh}}(\rho_{\text{sh}})d\rho_{\text{sh}} = \sum_i P(i)P(\rho_{\text{sh}}|i)d\rho_{\text{sh}}. \quad (4.3)$$

Our model predicts that the volume filling factor, $f_{V,\text{sh}} \equiv \sum_i P(i)$, is 29% ($r = 1$ kpc), 22% (8 kpc), 8.7% (50 kpc), 4.0% (100 kpc), and 1.2% (200 kpc), and these figures hardly change between CDM and SIDM. The remaining fraction, $1 - f_{V,\text{sh}}$, is in the smooth host-halo component. Following ref. [57], we model this host component as

$$P_{\text{h}}(\rho)d\rho = \frac{1 - f_{V,\text{sh}}}{\sqrt{2\pi}\Delta} \exp \left\{ -\frac{1}{2\Delta^2} \left[\ln \left(\frac{\rho}{\rho_0(r)} e^{\Delta^2/2} \right) \right]^2 \right\} \frac{d\rho}{\rho}, \quad (4.4)$$

where $\Delta = 0.2$. For $\rho_0(r)$, we adopt the NFW profile with $\rho_s = 0.245 \text{ GeV cm}^{-3}$, $r_s = 23.5$ kpc, which gives $\rho_0(8 \text{ kpc}) = 0.4 \text{ GeV cm}^{-3}$ for the local dark matter density around the solar system. Combining with the subhalo component from eq. (4.3), we have the total probability distribution function

$$P(\rho)d\rho = P_{\text{h}}(\rho)d\rho + P_{\text{sh}}(\rho - \rho_{\text{h}})d\rho. \quad (4.5)$$

We note that for obtaining the second term, we marginalise over the ρ_{h} following the probability density function, eq. (4.4).

In the top left panel of figure 7, we show $P(\rho)$ at the radius of the solar system, $r = 8$ kpc, comparing the cases of CDM and SIDM Model I. Although many low-mass subhalos experience core collapse with the SIDM parameters adopted, the probability for Earth to reside in such a collapsed region is so tiny that the effect does not appear as an enhancement in the density distribution $P(\rho)$. Instead, the suppression of the density profiles for cored higher-mass subhalos at larger radii in the SIDM case, as seen in figure 5, yields a more significant effect. This is because the larger fractional volume associated with these regions is of a more substantial impact. We also show the SIDM subhalo contributions from different mass ranges as dotted curves. The smaller subhalos are denser, but their overall contribution to the total density probability is more suppressed.

These findings, however, depend in detail on the SIDM model. In the top right panel of figure 7, we show $P(\rho)$ for the SIDM models I–V (table 1). In particular, SIDM Model III enhances the high-density tail of $P(\rho)$ compared to CDM due to the large collapse fraction for massive subhalos (figure 6, left panel). This is noteworthy because SIDM Model III can

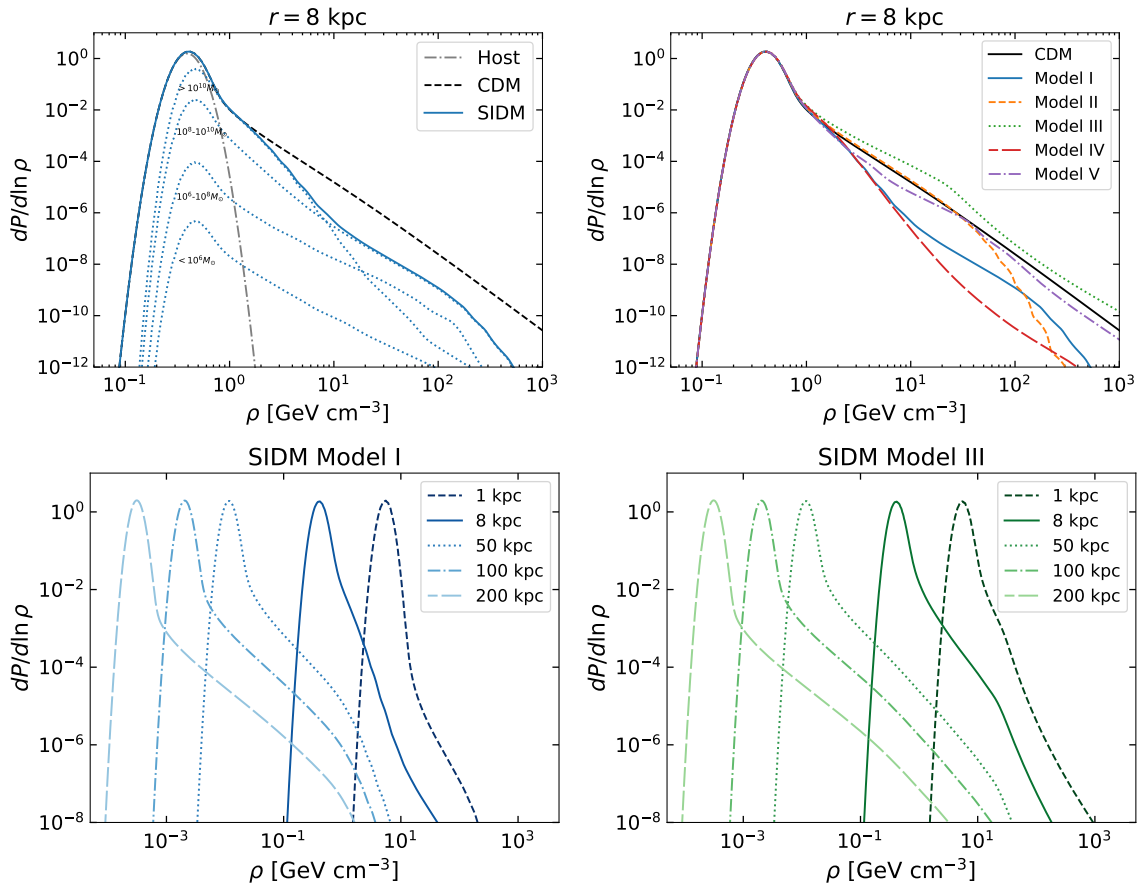


Figure 7. *Top left:* Probability distribution function of the local dark matter density $P(\rho)$ at 8 kpc from the host Milky-Way halo centre (dot-dashed), CDM subhalos and the halo (dashed) and SIDM (Model I; table 1) subhalos and the halo (solid). The dotted lines show contributions from the SIDM subhalos with masses larger than $10^{10} M_{\odot}$, between $10^{10} M_{\odot}$ and $10^8 M_{\odot}$, between $10^8 M_{\odot}$ and $10^6 M_{\odot}$, and smaller than $10^6 M_{\odot}$, from top to bottom at the left, respectively. *Top right:* The probability density function at 8 kpc (subhalos and the halo) for SIDM Models I–V (table 1) and CDM. *Bottom:* The probability density function of SIDM Model I (*left*) and Model III (*right*) at $r = 1, 8, 50, 100,$ and 200 kpc.

simultaneously explain astrophysical observations on a variety of scales [11, 60, 61] while affecting $P(\rho)$ in a distinct manner compared to the other SIDM models we study. Thus, there is an interplay between the SIDM cross section at different velocity scales and the local dark matter density, which both direct detection experiments and astrophysical probes of the Milky Way’s density profile may be sensitive to.

Finally, the bottom left (bottom right) panel of figure 7 compares the probability density function for SIDM Model I (Model III) at different radii. In both cases, the mean value of these distributions shifts to lower densities at larger radii, as expected because densities are lower in the outer regions of the host halo. Interestingly, the high-density tails of the distributions also become more pronounced at large radii, and this effect is stronger for Model III. It will be interesting to compare these predictions with cosmological zoom-in simulations in future work.

5 Conclusions

We have presented a new semi-analytical model, SASHIMI-SIDM, to efficiently predict SIDM subhalo populations down to arbitrarily low masses. By combining the structure-formation theory with a parametric model that connects the CDM subhalos to their SIDM counterpart, calibrated using the CDM and SIDM cosmological simulations, SASHIMI-SIDM runs in minutes without being limited by numerical resolution. Our main findings are as follows.

- By taking benchmark SIDM parameters with $\sigma_0/m_\chi = 147.1 \text{ cm}^2 \text{ g}^{-1}$ and $w = 24.33 \text{ km s}^{-1}$ in eq. (2.24), we compared the distribution of V_{max} (the maximum circular speed) and r_{max} (radius at which V_{max} is reached) with the results of the corresponding cosmological simulations, for the subhalos with masses heavier than $10^8 M_\odot/h$. We found good agreement for both the CDM and SIDM cases (figure 2).
- We then included subhalos with masses below the cosmological simulation’s resolution limit. For our fiducial SIDM model (Model I), the fraction of core-collapsed subhalos reaches its maximum of $\sim 30\%$ around subhalo masses of $10^7 M_\odot$, and the core-collapsed fraction decreases towards lower subhalo masses (figure 4).
- In the context of SASHIMI-SIDM, this behaviour can be explained by comparing the core-collapse timescale, and its dependence on V_{max} and r_{max} from eq. (2.23), to the age of the subhalo. We also provide an analytic understanding of the core-collapse fraction; see eq. (3.3) and the related discussion. Our predictions explain the behaviour of the core-collapsed fraction for various SIDM models (figure 6, left panel).
- We studied the implications for dark matter indirect-detection experiments. For our fiducial SIDM model (Model I), the rate of dark matter annihilation is enhanced by a factor of up to ~ 4 compared with the host-halo only expectation. This boost is further enhanced for SIDM models that reach larger cross sections at low relative velocities. For example, for Model II (table 1), the boost factor is as large as a factor of 10 (figure 6, right panel).
- We discussed the implications for local dark matter densities in the Milky Way. For SIDM Model I, even if a substantial fraction of the subhalos experience core-collapse, the total volume associated with these collapsed subhalos is tiny. Instead, we found the probability of finding a dense subhalo at the location of the solar system was decreased, compared to the CDM case, due to core formation of more massive subhalos (figure 7). This is, however, not the case for other models that predict larger fraction of collapsed subhalos (e.g., Model III).

Our finding that the core-collapse fraction peaks at a particular mass scale set by the underlying SIDM microphysics is particularly striking. For example, in our fiducial SIDM Model I from refs. [16, 27], which is motivated by the diverse rotation curves and inner densities of isolated dwarf galaxies and Milky Way satellites the core-collapse fraction peaks at present-day subhalo masses of $\sim 10^7 M_\odot$. Most of these low-mass subhalos fall into the Milky Way host recently, and reside at its outskirts; these systems are therefore not subject to strong tidal effects; it will be interesting to search for these systems in the outer Milky Way, both through their connection to the faintest dwarf galaxies and their impact on stellar streams in the outer halo. Meanwhile, SIDM Model III, which is motivated by observations of low-concentration ultra-diffuse galaxies and extremely dense strong gravitational lensing

perturbors [11], the core-collapse fraction peaks at higher subhalo masses of $\sim 10^9\text{--}10^{10}M_\odot$. Our analytic calculation of the core-collapsed fraction highlights that this result is sensitive to the assumed mass-concentration relation, which should be studied in SIDM models at very low subhalo masses.

We have demonstrated that SASHIMI-SIDM can rapidly and accurately generate SIDM subhalo populations down to arbitrarily low masses. This will enable more comprehensive and efficient scans of SIDM parameter space, allowing these models to be tested using astronomical data. Relevant observables include dwarf galaxy number counts and density profiles [62, 63], strong gravitational lensing flux ratio statistics and gravitational imaging data [64], stellar stream perturbations [65], and pulsar timing array signals [66]. These can be probed with current and future facilities such as the James Webb Space Telescope [67], Euclid [68], the Vera C. Rubin Observatory [69], and the Nancy Grace Roman Space Telescope [70]. We plan to pursue these tests of SIDM in future studies.

Acknowledgments

This work was supported by MEXT KAKENHI under grant numbers JP20H05850 (SA) and JP20H05861 (SA and SH), the John Templeton Foundation under grant ID #61884 and the U.S. Department of Energy under grant number de-sc0008541 (DY and HBY). We thank the Pollica Physics Center, where this research was initiated, for its warm hospitality. The Pollica Physics Center is supported by the Regione Campania, Università degli Studi di Salerno, Università degli Studi di Napoli “Federico I,” the Physics Department “Ettore Pancini” and “E.R. Caianiello,” and the Istituto Nazionale di Fisica Nucleare.

References

- [1] J.S. Bullock and M. Boylan-Kolchin, *Small-Scale Challenges to the Λ CDM Paradigm*, *Ann. Rev. Astron. Astrophys.* **55** (2017) 343 [1707.04256].
- [2] F. Nesti, P. Salucci and N. Turini, *The Quest for the Nature of the Dark Matter: The Need of a New Paradigm*, *Astronomy* **2** (2023) 90 [2308.02004].
- [3] D.N. Spergel and P.J. Steinhardt, *Observational evidence for selfinteracting cold dark matter*, *Phys. Rev. Lett.* **84** (2000) 3760 [astro-ph/9909386].
- [4] S. Tulin and H.-B. Yu, *Dark Matter Self-interactions and Small Scale Structure*, *Phys. Rept.* **730** (2018) 1 [1705.02358].
- [5] S. Adhikari et al., *Astrophysical Tests of Dark Matter Self-Interactions*, 2207.10638.
- [6] J.F. Navarro, C.S. Frenk and S.D.M. White, *The Structure of cold dark matter halos*, *Astrophys. J.* **462** (1996) 563 [astro-ph/9508025].
- [7] S. Balberg, S.L. Shapiro and S. Inagaki, *Selfinteracting dark matter halos and the gravothermal catastrophe*, *Astrophys. J.* **568** (2002) 475 [astro-ph/0110561].
- [8] J. Koda and P.R. Shapiro, *Gravothermal collapse of isolated self-interacting dark matter haloes: N-body simulation versus the fluid model*, *Mon. Not. Roy. Astron. Soc.* **415** (2011) 1125 [1101.3097].
- [9] R. Essig, S.D. McDermott, H.-B. Yu and Y.-M. Zhong, *Constraining Dissipative Dark Matter Self-Interactions*, *Phys. Rev. Lett.* **123** (2019) 121102 [1809.01144].
- [10] M. Kaplinghat, M. Valli and H.-B. Yu, *Too Big To Fail in Light of Gaia*, *Mon. Not. Roy. Astron. Soc.* **490** (2019) 231 [1904.04939].

- [11] E.O. Nadler, D. Yang and H.-B. Yu, *A Self-interacting Dark Matter Solution to the Extreme Diversity of Low-mass Halo Properties*, *Astrophys. J. Lett.* **958** (2023) L39 [2306.01830].
- [12] A. Kamada, M. Kaplinghat, A.B. Pace and H.-B. Yu, *How the Self-Interacting Dark Matter Model Explains the Diverse Galactic Rotation Curves*, *Phys. Rev. Lett.* **119** (2017) 111102 [1611.02716].
- [13] T. Ren, A. Kwa, M. Kaplinghat and H.-B. Yu, *Reconciling the Diversity and Uniformity of Galactic Rotation Curves with Self-Interacting Dark Matter*, *Phys. Rev. X* **9** (2019) 031020 [1808.05695].
- [14] O. Sameie, H.-B. Yu, L.V. Sales, M. Vogelsberger and J. Zavala, *Self-Interacting Dark Matter Subhalos in the Milky Way's Tides*, *Phys. Rev. Lett.* **124** (2020) 141102 [1904.07872].
- [15] C.A. Correa, *Constraining velocity-dependent self-interacting dark matter with the Milky Way's dwarf spheroidal galaxies*, *Mon. Not. Roy. Astron. Soc.* **503** (2021) 920 [2007.02958].
- [16] H.C. Turner, M.R. Lovell, J. Zavala and M. Vogelsberger, *The onset of gravothermal core collapse in velocity-dependent self-interacting dark matter subhaloes*, *Mon. Not. Roy. Astron. Soc.* **505** (2021) 5327 [2010.02924].
- [17] C.A. Correa, M. Schaller, S. Ploekinger, N. Anau Montel, C. Weniger and S. Ando, *TangoSIDM: Tantalizing models of Self-Interacting Dark Matter*, *Mon. Not. Roy. Astron. Soc.* **517** (2022) 3045 [2206.11298].
- [18] D. Yang, E.O. Nadler, H.-B. Yu and Y.-M. Zhong, *A parametric model for self-interacting dark matter halos*, *JCAP* **02** (2024) 032 [2305.16176].
- [19] H. Nishikawa, K.K. Boddy and M. Kaplinghat, *Accelerated core collapse in tidally stripped self-interacting dark matter halos*, *Phys. Rev. D* **101** (2020) 063009 [1901.00499].
- [20] F. Kahlhoefer, M. Kaplinghat, T.R. Slatyer and C.-L. Wu, *Diversity in density profiles of self-interacting dark matter satellite halos*, *JCAP* **12** (2019) 010 [1904.10539].
- [21] Z.C. Zeng, A.H.G. Peter, X. Du, A. Benson, S. Kim, F. Jiang et al., *Core-collapse, evaporation, and tidal effects: the life story of a self-interacting dark matter subhalo*, *Mon. Not. Roy. Astron. Soc.* **513** (2022) 4845 [2110.00259].
- [22] D. Yang and H.-B. Yu, *Self-interacting dark matter and small-scale gravitational lenses in galaxy clusters*, *Phys. Rev. D* **104** (2021) 103031 [2102.02375].
- [23] M. Shirasaki, T. Okamoto and S. Ando, *Modelling self-interacting dark matter substructures – I. Calibration with N-body simulations of a Milky-Way-sized halo and its satellite*, *Mon. Not. Roy. Astron. Soc.* **516** (2022) 4594 [2205.09920].
- [24] H. Meskhidze, F.J. Mercado, O. Sameie, V.H. Robles, J.S. Bullock, M. Kaplinghat et al., *Comparing implementations of self-interacting dark matter in the gizmo and arepo codes*, *Mon. Not. Roy. Astron. Soc.* **513** (2022) 2600 [2203.06035].
- [25] I. Palubski, O. Slone, M. Kaplinghat, M. Lisanti and F. Jiang, *Numerical Challenges in Modeling Gravothermal Collapse in Self-Interacting Dark Matter Halos*, **2402.12452**.
- [26] M.S. Fischer, K. Dolag and H.-B. Yu, *Numerical challenges for energy conservation in N-body simulations of collapsing self-interacting dark matter haloes*, **2403.00739**.
- [27] D. Yang, E.O. Nadler and H.-B. Yu, *Strong Dark Matter Self-interactions Diversify Halo Populations within and surrounding the Milky Way*, *Astrophys. J.* **949** (2023) 67 [2211.13768].
- [28] N. Hiroshima, S. Ando and T. Ishiyama, *Modeling evolution of dark matter substructure and annihilation boost*, *Phys. Rev. D* **97** (2018) 123002 [1803.07691].
- [29] S. Ando, A. Geringer-Sameth, N. Hiroshima, S. Hoof, R. Trotta and M.G. Walker, *Structure formation models weaken limits on WIMP dark matter from dwarf spheroidal galaxies*, *Phys. Rev. D* **102** (2020) 061302 [2002.11956].

- [30] J.R. Bond, S. Cole, G. Efstathiou and N. Kaiser, *Excursion set mass functions for hierarchical Gaussian fluctuations*, *Astrophys. J.* **379** (1991) 440.
- [31] X. Yang, H.J. Mo, Y. Zhang and F.C.v.d. Bosch, *An analytical model for the accretion of dark matter subhalos*, *Astrophys. J.* **741** (2011) 13 [[1104.1757](#)].
- [32] C.A. Correa, J.S.B. Wyithe, J. Schaye and A.R. Duffy, *The accretion history of dark matter haloes – I. The physical origin of the universal function*, *Mon. Not. Roy. Astron. Soc.* **450** (2015) 1514 [[1409.5228](#)].
- [33] G.L. Bryan and M.L. Norman, *Statistical properties of x-ray clusters: Analytic and numerical comparisons*, *Astrophys. J.* **495** (1998) 80 [[astro-ph/9710107](#)].
- [34] C.A. Correa, J.S.B. Wyithe, J. Schaye and A.R. Duffy, *The accretion history of dark matter haloes – III. A physical model for the concentration–mass relation*, *Mon. Not. Roy. Astron. Soc.* **452** (2015) 1217 [[1502.00391](#)].
- [35] T. Ishiyama, J. Makino, S. Portegies Zwart, D. Groen, K. Nitadori, S. Rieder et al., *The Cosmogrid Simulation: Statistical Properties of Small Dark Matter Halos*, *Astrophys. J.* **767** (2013) 146 [[1101.2020](#)].
- [36] J. Penarrubia, A.J. Benson, M.G. Walker, G. Gilmore, A. McConnachie and L. Mayer, *The impact of dark matter cusps and cores on the satellite galaxy population around spiral galaxies*, *Mon. Not. Roy. Astron. Soc.* **406** (2010) 1290 [[1002.3376](#)].
- [37] E.O. Nadler, A. Banerjee, S. Adhikari, Y.-Y. Mao and R.H. Wechsler, *Signatures of Velocity-Dependent Dark Matter Self-Interactions in Milky Way-mass Halos*, *Astrophys. J.* **896** (2020) 112 [[2001.08754](#)].
- [38] J. Pollack, D.N. Spergel and P.J. Steinhardt, *Supermassive Black Holes from Ultra-Strongly Self-Interacting Dark Matter*, *Astrophys. J.* **804** (2015) 131 [[1501.00017](#)].
- [39] S. Yang, X. Du, Z.C. Zeng, A. Benson, F. Jiang, E.O. Nadler et al., *Gravothermal Solutions of SIDM Halos: Mapping from Constant to Velocity-dependent Cross Section*, *Astrophys. J.* **946** (2023) 47 [[2205.02957](#)].
- [40] D. Yang and H.-B. Yu, *Gravothermal evolution of dark matter halos with differential elastic scattering*, *JCAP* **09** (2022) 077 [[2205.03392](#)].
- [41] D. Gilman, J. Bovy, T. Treu, A. Nierenberg, S. Birrer, A. Benson et al., *Strong lensing signatures of self-interacting dark matter in low-mass haloes*, *Mon. Not. Roy. Astron. Soc.* **507** (2021) 2432 [[2105.05259](#)].
- [42] M. Kaplinghat, S. Tulin and H.-B. Yu, *Dark Matter Halos as Particle Colliders: Unified Solution to Small-Scale Structure Puzzles from Dwarfs to Clusters*, *Phys. Rev. Lett.* **116** (2016) 041302 [[1508.03339](#)].
- [43] K.E. Andrade, J. Fuson, S. Gad-Nasr, D. Kong, Q. Minor, M.G. Roberts et al., *A stringent upper limit on dark matter self-interaction cross-section from cluster strong lensing*, *Mon. Not. Roy. Astron. Soc.* **510** (2021) 54 [[2012.06611](#)].
- [44] N.J. Outmezzguine, K.K. Boddy, S. Gad-Nasr, M. Kaplinghat and L. Sagunski, *Universal gravothermal evolution of isolated self-interacting dark matter halos for velocity-dependent cross sections*, [2204.06568](#).
- [45] H. Zheng, S. Bose, C.S. Frenk, L. Gao, A. Jenkins, S. Liao et al., *The abundance of dark matter haloes down to Earth mass*, [2310.16093](#).
- [46] W.-X. Feng, H.-B. Yu and Y.-M. Zhong, *Seeding Supermassive Black Holes with Self-interacting Dark Matter: A Unified Scenario with Baryons*, *Astrophys. J. Lett.* **914** (2021) L26 [[2010.15132](#)].

- [47] N. Shah and S. Adhikari, *The abundance of core-collapsed subhalos in SIDM: insights from structure formation in Λ CDM*, [2308.16342](#).
- [48] S. Tulin, H.-B. Yu and K.M. Zurek, *Beyond Collisionless Dark Matter: Particle Physics Dynamics for Dark Matter Halo Structure*, *Phys. Rev. D* **87** (2013) 115007 [[1302.3898](#)].
- [49] Y. Wu, S. Baum, K. Freese, L. Visinelli and H.-B. Yu, *Dark stars powered by self-interacting dark matter*, *Phys. Rev. D* **106** (2022) 043028 [[2205.10904](#)].
- [50] M. Kaplinghat, R.E. Keeley, T. Linden and H.-B. Yu, *Tying Dark Matter to Baryons with Self-interactions*, *Phys. Rev. Lett.* **113** (2014) 021302 [[1311.6524](#)].
- [51] O. Sameie, P. Creasey, H.-B. Yu, L.V. Sales, M. Vogelsberger and J. Zavala, *The impact of baryonic discs on the shapes and profiles of self-interacting dark matter haloes*, *Mon. Not. Roy. Astron. Soc.* **479** (2018) 359 [[1801.09682](#)].
- [52] V.H. Robles, T. Kelley, J.S. Bullock and M. Kaplinghat, *The Milky Way's halo and subhaloes in self-interacting dark matter*, *Mon. Not. Roy. Astron. Soc.* **490** (2019) 2117 [[1903.01469](#)].
- [53] J.C. Rose, P. Torrey, M. Vogelsberger and S. O'Neil, *Unravelling the interplay between SIDM and baryons in MW haloes: defining where baryons dictate heat transfer*, *Mon. Not. Roy. Astron. Soc.* **519** (2023) 5623 [[2206.14830](#)].
- [54] S. Ando, T. Ishiyama and N. Hiroshima, *Halo Substructure Boosts to the Signatures of Dark Matter Annihilation*, *Galaxies* **7** (2019) 68 [[1903.11427](#)].
- [55] S. Horigome, K. Hayashi and S. Ando, *Cosmological prior for the J-factor estimation of dwarf spheroidal galaxies*, *Phys. Rev. D* **108** (2023) 083530 [[2207.10378](#)].
- [56] M. Kamionkowski and S.M. Koushiappas, *Galactic substructure and direct detection of dark matter*, *Phys. Rev. D* **77** (2008) 103509 [[0801.3269](#)].
- [57] M. Kamionkowski, S.M. Koushiappas and M. Kuhlen, *Galactic Substructure and Dark Matter Annihilation in the Milky Way Halo*, *Phys. Rev. D* **81** (2010) 043532 [[1001.3144](#)].
- [58] A. Ibarra, B.J. Kavanagh and A. Rappelt, *Impact of substructure on local dark matter searches*, *JCAP* **12** (2019) 013 [[1908.00747](#)].
- [59] V. Springel, J. Wang, M. Vogelsberger, A. Ludlow, A. Jenkins, A. Helmi et al., *The Aquarius Project: the subhalos of galactic halos*, *Mon. Not. Roy. Astron. Soc.* **391** (2008) 1685 [[0809.0898](#)].
- [60] X. Zhang, H.-B. Yu, D. Yang and H. An, *Self-interacting dark matter interpretation of Crater II*, [2401.04985](#).
- [61] D. Kong, D. Yang and H.-B. Yu, *CDM and SIDM Interpretations of the Strong Gravitational Lensing Object JWST-ER1*, [2402.15840](#).
- [62] J.D. Simon et al., *Dynamical Masses for a Complete Census of Local Dwarf Galaxies*, [1903.04743](#).
- [63] E.O. Nadler, V. Gluscevic, T. Driskell, R.H. Wechsler, L.A. Moustakas, A. Benson et al., *Forecasts for Galaxy Formation and Dark Matter Constraints from Dwarf Galaxy Surveys*, [2401.10318](#).
- [64] S. Vegetti et al., *Strong gravitational lensing as a probe of dark matter*, [2306.11781](#).
- [65] N. Banik, G. Bertone, J. Bovy and N. Bozorgnia, *Probing the nature of dark matter particles with stellar streams*, *JCAP* **07** (2018) 061 [[1804.04384](#)].
- [66] H. Ramani, T. Trickle and K.M. Zurek, *Observability of Dark Matter Substructure with Pulsar Timing Correlations*, *JCAP* **12** (2020) 033 [[2005.03030](#)].
- [67] J.P. Gardner et al., *The James Webb Space Telescope*, *Space Sci. Rev.* **123** (2006) 485 [[astro-ph/0606175](#)].

- [68] EUCLID collaboration, *Euclid preparation. I. The Euclid Wide Survey*, *Astron. Astrophys.* **662** (2022) A112 [[2108.01201](#)].
- [69] LSST collaboration, *LSST: from Science Drivers to Reference Design and Anticipated Data Products*, *Astrophys. J.* **873** (2019) 111 [[0805.2366](#)].
- [70] D. Spergel et al., *Wide-Field InfrarRed Survey Telescope-Astrophysics Focused Telescope Assets WFIRST-AFTA 2015 Report*, [1503.03757](#).